An Amplification Shaping Framework for Exoskeletal Human Strength Augmentation

Gray Cortright Thomas, *Member, IEEE,* Orion Campbell IV, *Student Member, IEEE,* Nick Nichols, Nicholas Brissoneau, *Student Member, IEEE,* Binghan He, *Student Member, IEEE,* Joshua James, Nicholas Paine, *Member, IEEE,* and Luis Sentis, *Member, IEEE*

***Abstract*—Augmenting the physical strength of a human operator during unpredictable human-directed (volitional) movements is a relevant capability for several proposed exoskeleton applications, including mobility augmentation, manual material handling, tool operation, and mounting useful payloads. Unlike controllers and augmentation systems designed for repetitive tasks (e.g. walking), we approach physical strength augmentation by a task-agnostic method of force amplification—using force/torque sensors at the human–machine interface to estimate the human task force, and then amplifying it with the robot. Coupled stability of the machine with the human motivates our introduction of an amplification shaping framework for the design of safe controllers. To avoid system identification of the operator wearing the exoskeleton, we refine the amplification strategy down to a one-parameter tunable compensator. This amplification controller is integrated into a complete framework for controlling exoskeletons which includes human-led foot transitions, inequality constraints, and a computationally efficient prioritization. A powered lower-body exoskeleton is used to demonstrate behavior of the control framework in a lab environment.**

I. Introduction

EXOSKELETONS are a broad category of wearable robotics with many potential applications. Some aim to recover locomotion capability lost to disease [1], [2], or to offload the strenuous work of rehabilitation therapy from therapists [3], [4]. Others aim to improve mobility of healthy operators by augmenting their motion with simple pre-programmed boosts [5]. Exosuits (exoskeletons without rigid structures) have also seen some notable success in this area [6]. Also concerning healthy operators, [7] defines "capability platform" applications as ones where the exoskeleton lifts relevant (and well modeled) payloads, like body armor, cooling systems, or tools. The related applications of manual material handling, and tool operation differ in that they do not have well understood payloads—in these applications the exoskeleton is expected to improve the user's physical strength as they manipulate the unknown environment. This paper focuses on amplification control systems designed to magnify the physical strength of operators as they attempt non-repetitive, unpredictable tasks. This focus extends beyond the hardware we employ, which was designed to consider only the capability platform application (though it has the force sensing needed to test amplification control systems).

Ref. [8] employs a distinction between "human-in-the-loop" systems, where humans provide the final OK on actions and "human-on-the-loop" systems where humans take on a more abstracted managerial intervention role. Clearly, exoskeletons provide much more direct control for the human (perhaps requiring that the "human-is-the-loop"). But even within exoskeleton control, amplification is very low-level. In the general controller framework of [9], all exoskeleton control can be split into low (joint state implementation), middle (intent to state), and high level (intent recognition) control layers. Amplification control distinguishes itself in having a trivial high level layer, as opposed to systems which must classify human intent into action types [10]. It also has a relatively straightforward middle layer—a whole body task controller—which requires far less optimization and tuning than approaches which use a lookup table or adjustable functions to assign torques based on perceived completion of the gait cycle [6], [5].

Other "human-is-the-loop" approaches to exoskeleton control have been used for purposes besides amplification of human strength. Apparent inertia of the operator [11] or the exoskeleton [12] can be reduced through feedback of acceleration. The BLEEX exoskeleton also employs a combination of gravity compensation and positive acceleration feedback to attenuate the operator's perception of known loads [13], [12]. The operator's own weight can also be compensated for using an operator model [14] or "potential energy shaping" of the exoskeleton–human system [15], [16]. While all of these can be accomplished using high fidelity sensing of position or force, more ambitious sensing approaches have also proliferated thanks to low-cost sensors of human muscle activation [17], [18].

In heavy exoskeletons, gravity compensation of the weight of the exoskeleton itself can be the largest responsibility of the controller [13]. This requires a decent model of the exoskeleton mass, however this requirement can be avoided by using low level position control and cascaded high level

G. Thomas, B. He, N. Brissoneau were with the Department of Mechanical Engineering, University of Texas at Austin, Austin, TX, 78712 USA (G. Thomas's e-mail: gcthomas@umich.edu).

L. Sentis was with The department of Aerospace Engineering, University of Texas at Austin, Austin, TX, 78712 USA (e-mail: lsentis@austin.utexas.edu).

O. Campbell, N. Nichols, J. James, and N. Paine were with Appronik Systems, Inc., Austin, TX, 78758 USA.

Manuscript not yet submitted September 6, 2019; nor revised.

Color versions of one or more of the figures in this paper are available online at https://ieeexplore.ieee.org.

Digital Object Identifier XX.XXXX/SRO.2019.XXXXXXX

force control, a strategy known as admittance control [19], [20], [21]. Gravity compensation is the majority of the task for a capability platform system, but only part of the task for manual materials handling and tool operation. The other component being the augmentation of the forces the system applies to the unknown environment or manipulated object.

The earliest attempt at human strength amplification with a powered exoskeleton, HARDIMAN I, used joint-level feedback and a hydraulic actuation system that forced a roughly 25 to 1 strength amplification ratio—the area ratio between the two actuation cylinders on the load-side and human-side structures [22]. This strategy was reported to be successful on the upper body, but unstable on the lower body (perhaps due to the independent joint controllers neglecting coupling effects). The concept of an extender is based on a similar, but better implemented, concept of different human-side and environment-side behavior [23], using a position controlled robot and dictating the desired motion resulting from either kind of measured force explicitly (using one sensor for the human and another for the environment). This extender strategy extended to 2D [24], [25], and a giant six-DOF crab-claw arm [26]. In all cases the stability analysis for the extender depended on models for both the environment and the human, and took advantage of the non-backdrivable low-level system. An important feature of this research is that the strength amplification ratio is equivalent to the ratio between the human side admittance and the environment side admittance of the exoskeleton—a point we will elaborate on using compliance (position per force) in place of admittance (velocity per force) transfer functions.

The strength amplification claim of the extender system rests on the two force sensors distinguishing human inputs from the environment. Without the environment-side sensing, the strategy is called admittance control. With no force-feedback to make the environment-side port of the exoskeleton more compliant than the low-level position controller, admittance control is more of a feedforward system from the human point of view. (Transmission friction in the drivetrain of a position controlled system typically makes it much less backdrivable than a linear model would suggest.) The SARCOS/Raytheon exoskeleton (responsible for some of the most impressive strength amplification footage to date) appears to have used the admittance control strategy, according to their patent [21], to achieve a "get out of the way" behavior where the robot responsively moves away from detected interaction forces. The strategy lends itself well to large (or strongly position controlled) robots where the human cannot move the robot by themselves [27], at which point the force sensor functions almost like a joystick control for the robot. Ref. [19] emphasizes the importance of quality, model-free, position control at the mid level in the application of admittance control. Similarly, the Body Extender [20] (not to be confused with the human extender introduced in [26]), which is a heavy-duty exoskeleton designed for manual materials handling applications, has a controller that allows for a desired robot impedance transfer function, but (as with the others) leaves the selection of this impedance beyond the scope of the paper.

As shown in [28], low level position feedback controllers can be entirely cancelled out by high-level control if the high level control desires a compliant behavior. But this is accomplished by additional high level position feedback. Since the admittance control strategy does not do this, it ultimately reduces the compliance of the environment-side port of the exoskeleton. Low level force control is a more direct way to achieve backdrivability of the environment-side of the exoskeleton, for example by employing series elastic actuators with force disturbance observers [29], [30]. A backdrivable system with gravity compensation may well be sufficient for a capability platform application [31]. To improve the human experience relative to such a backdrivable, gravity-compensated system, a controller must—either by positive acceleration feedback [12], or by interface force feedback (this paper)—increase the compliance of the human interface.

However, there are limits on the ability of a system to alter the behavior it presents at the human interface, since the coupled human–exoskeleton system must be stable [23]. As discussed in the literature on haptic impedance rendering, the human is hard to model accurately and requires controllers which are robust to the variation in its potential behavior [32], [33], [34], [35]. More specificially, it is the operator's natural (and unconscious) high frequency dynamics—indirectly adjustable with antagonistic muscle co-contraction [36]—that are important to model in order to avoid resonance that the human does not want or expect. While many interaction controllers treat the space of possible unconscious user impedances as the set of all passive impedances, this is a very conservative assumption which severely limits performance [37]. A recent and more accurate representation of human behavior is that of a complex stiffness (with an inertia at higher frequencies) [38]. Using this model with parameteric uncertainty in the spring stiffness and damping ratio, stable amplification systems can be designed using robust control[39] or by shaping the compliance [40]. Both of these last strategies are tested only on a one-degree of freedom system, which permits extensive system identification and careful design. Ref. [39]'s controller also suffered from a lack of analytical guarantees about what behavior would be accomplished. And [40] presented a very complex strategy that depended on re-implementing the series elastic actuator controller at the high level in a way that changed its behavior as a function of the joint inertia (i.e. the mass matrix).

However, for an amplification controller that could be scaled up to a real exoskeleton, this type of extensive system identification of the human operator is impractical—especially since these models need to be robust against so many experimental conditions. Additionally, these works exploited a fixed based, and did not present a complete strategy that handles inequality constraints due to torque limits and the multi-contact nature of a lower body exoskeleton.

In this paper, we present a comprehensive framework for achieving amplification control in exoskeletons that is based on force-sensor feedback and increases the compliance of the human interface. Our frequency-domain amplification shaping control strategy distills the complex approaches of [39] and [40] down to a single parameter tuning problem (per amplified task). The framework includes foot contacts, inequality

Fig. 1. The Apptronik Sagittarius Exoskeleton used in this paper. The operator can climb stairs with the exoskeleton, even when it is not amplifying forces, due to the backdrivable force controlled actuators (gravity compensation and strength amplification are both active in the pictured movement). Coloring segregates rigid exoskeleton parts for the right leg (blue-through-purple), human interfaces (orange) and the safety features (red).

constraints, and computationally efficient prioritization of the tasks.

II. Theory of Strength Amplification Tasks

TABLE I
Nomenclature for Sec. II

Symbol	Meaning
M_e, B_e, g_e	exoskeleton mass, Coriolis, gravity
$\ddot{q}$, $\dot{q}$, q	joint acceleration, velocity, position
τ	joint torque vector
J_c, f_c	human interaction cuff Jacobian, forces
J_e, f_e	environment interaction Jacobian, forces
J_t	task jacobian
$\bar{J}_t$	dynamically consistant pseudo-inverse of J_t
x_t	task position
$\hat{f}_t$	desired task force
α	amplification rate

In this section we introduce an ideal strength amplification behavior as a task for a redundant robot. This represents the ideal behavior in the sense that it is an unimplementable control law that requires unlimited control bandwidth. It serves to demonstrate some properties of the amplification behavior.

Consider a fully actuated, grounded base exoskeleton robot in contact with both a human operator (Jacobian J_c, and force f_c) and an environment (Jacobian J_e, and force f_e), using the notational system laid out in Tab. I,

$$M_e\ddot{q} + B_e + g_e = \tau + J_c^T f_c + J_e^T f_e, \tag{1}$$

where the environment and the human are acting as inputs to the system, and the joint torque vector τ will be partially specified in terms of the measured human torque. We are interested in the way the human perceives the environment once the controller has been defined—we want to define a control which increases the magnitude of the human forces relative to the magnitude of the environmental forces within the context of the task.

Looking at the task space,

$$\Lambda_t(\ddot{x}_t - \dot{J}_t\dot{q}) + \bar{J}_t^T(B_e + g_e) = \bar{J}_t^T(\tau + J_c^T f_c + J_e^T f_e), \tag{2}$$

where $\Lambda_t = (J_t M_e^{-1} J_t^T)^{-1}$ is the operational space mass matrix and $\bar{J}_t = M_e^{-1} J_t^T \Lambda_t$ is the dynamically consistent pseudo-inverse of the task Jacobian.

Specifying the new behavior in only this task, we define the ideal amplificaiton task law as

$$\bar{J}_t^T \tau = (\alpha - 1)\bar{J}_t^T J_c^T f_c + \bar{J}_t^T(g_e), \tag{3}$$

where the first term represents amplification of the human operator's influence on the task, and the second term removes the gravity bias.

With this controller,

$$\Lambda_t(\ddot{x}_t - \dot{J}_t\dot{q}) + \bar{J}_t^T(B_e) = \alpha\bar{J}_t^T J_c^T f_c + \bar{J}_t^T J_e^T f_e, \tag{4}$$

which clearly amplifies the influence of the human force by a factor of α, but is complicated due to the potential mismatch between the task definition, the human cuff locations, and the location of any environmental forces. If we assume that these three are all the same—for example if all three are applied to one end effector and, to use the spatial force vector concept from [41], the spatial forces f_c and f_e are both expressed in the task frame—such that $J_t = J_c = J_e$, then we can observe amplification behavior as defined below.

Definition 1 (Ideal Amplification Behavior)**.** When the operational space dynamics of a task are unchanged, except that the strength of the human is multiplied by a scalar $\alpha > 1$, as in

$$\Lambda_t(\ddot{x}_t - \dot{J}_t\dot{q}) + \bar{J}_t^T(B_e) = \alpha f_c + f_e, \tag{5}$$

we say the human is experiencing ideal amplification in that task-frame.

This control gives the human a clear advantage, both with respect to external forces and with respect to the dynamics of the exoskeleton itself as perceived by the operator. We can also see that the x_t solutions to the above differential equation, if we assume it is linear[1], is the sum of the solutions for the two inputs (f_c and f_e) independently. The amplification factor α can therefore also be thought of as magnifying the

[1]As would be very nearly the case if the magnitude of motion was small, the velocity was near zero, and the robot was far from any singularities.

amount of motion generated by the human forces (as measured using the human interaction sensor values, or "cuff forces") as compared to external forces. And this leads us to define amplification as the ratio of compliance transfer functions between the larger human-side compliance and the smaller environment-side compliance.

This concept of amplification matches that of [26], but describes it using robot dynamics free from a position controller. This highlights the backdrivable control foundation of our approach: the exoskeleton can be moved freely by the operator, and the amplification serves to mask some of the inertia and attenuate the external forces that an operator feels. The degrees of freedom in which this behavior occurs are controlled by the placement of the amplification tasks. Different degrees of freedom of the exoskeleton need not share an amplification rate (though this could distort the human perception of external forces). And the task definition mechanics allows these degrees of freedom to be expressed arbitrarily (not restricted, for example, to the joint space of the robot or the operator).

We call this law ideal because this law changes the apparent inertia the human feels instantaneously—which is quite a simplification. In the frequency domain, this is equivalent to claiming that the compliance of the human is higher at all frequencies and that the actuation which renders a magnification of the sensor force suffers no phase lag from either time delay or low level bandwidth limitations.

III. Shaping Amplification in the Frequency Domain

TABLE II
NOMENCLATURE FOR SEC. III

Symbol	Meaning
$C_H(s)$	c.l. human-side compliance
$H(s)$	human compliance
K_h	human stiffness
ϕ	human phase lag
M	mass
$x(t)$, $X(s)$	position
$f_E(t)$, $F_E(s)$	environmental force
$f_A(t)$, $F_A(s)$	actuation force
$f_H(t)$, $F_H(s)$	human force
$\hat{\alpha}(s)$	desired amplification
$\alpha(s)$	realized amplification
$K(s)$	feedback controller
$C_E(s)$	environment-side compliance
$C_A(s)$	compliance w.r.t. actuation command
$\eta(s)$	actuation imperfections

A. Compliance Shaping

Compliances are transfer functions representing position per force—expressing the same information as admittance or impedance which are velocity per force and force per velocity respectively. Shaping the amplification ratio without changing the backdrivable environment-side compliance is equivalent to shaping the human-side compliance. To help us in this task we draw upon a set of Bode plot tools (collectively known as the compliance shaping approach) which will allow us to design a compliance which will be stable when rigidly attached to the human operator.

The reason we use compliance transfer functions and not admittance or impedance transfer functions, is to highlight the relationship between the system in parallel with a spring and the frequency domain design method for proportional feedback (as in [42] Chapter 6) [43], [40]. A compliance under proportional feedback has a controller with units of force per position—a spring. Thus, if we consider a compliance under proportional feedback using the Bode plot crossover point / phase margin technique to analyze stability, we are equivalently analyzing its stability with respect to linear springs. A more general phase margin concept could be applied to other representations of the system transfer function, but compliance plots stay closest to the textbook examples in that the feedback is proportional and the result is a low pass filter.

Passive systems require energy input to maintain periodic motions, which occurs when the integration of mechanical work (force times velocity) is positive over the motion. The sign of this integral can be found by comparing the phase of the force and velocity signals for sinusoidal signals. And because of this there is a direct link between the phase of a transfer function relating force and velocity (or position) and the passivity of the system it represents. For admittance or impedance transfer functions, the system is passive if the transfer function is positive real. Since compliance is just admittance divided by s, the passive phase region shifts by $-90°$. Thus compliances are passive if their phase is in the range $-180°$ to $0°$—the negative imaginary range.

Since the human behaves similarly to a spring, we can use the phase margin of the compliance of the exoskeleton's human interface to determine coupled stability with the human. But humans are not quite perfect springs, and this is a fairly conservative test. The complex stiffness model introduced in [38] offers a more accurate model where the human dissipates energy. This complex stiffness model treats the human as a spring with a constant frequency-domain phase lag to represent the non-linear damping properties of the human. The model is explicitly only a frequency domain model, but the behavior is similar to what might be achieved with coulomb friction that scales with the spring force magnitude. We do not model the inertial behavior of the human.

Because our human model includes some energy-dissipating phase lag, it is easier to achieve coupled stability with humans than with perfect springs. To represent this distinction, we introduce the 'Human Phase Margin.'

Definition 2. A compliance $C_H(s)$ in parallel with a complex human compliance $H(s) = K_h^{-1} e^{\frac{\pi}{180}\phi j}$ with $-90° < \phi < 0$ which intersects at a "human crossover frequency" ω such that $\|H(j\omega)\| = \|C_H(j\omega)\|$ has a "human phase margin" equal to $\angle C_H(j\omega) + \phi - 180°$.

Rather than comparing compliance phase $\angle C(j\omega)$ to a $-180°$ reference, as in the traditional phase margin, the human phase margin compares it to a $\phi - 180°$ reference, where ϕ is the phase lag of the human's complex spring. This concept is closely related to the phase-based passivity relaxations in [40], [43] in that systems which are relaxed-phase passive within ϕ

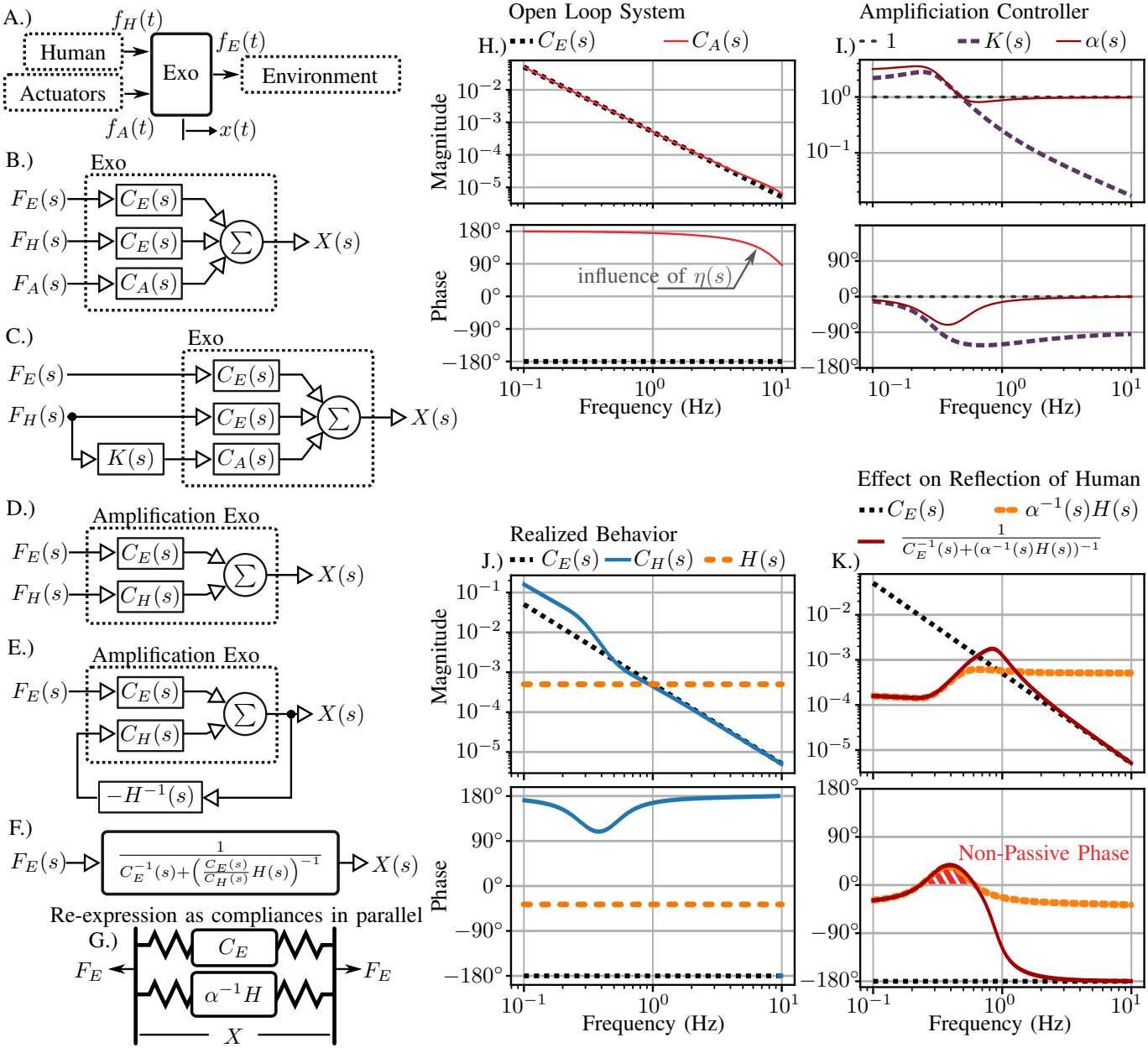

Fig. 2. Block diagrams and Bode plots explaining the controller. A.) Three forces acting on the inertia of the exoskeleton in a one dimensional model. B.) This model represented as a block diagram with three inputs and one output. C.) The addition of amplification control (controller $K(s)$) to the exoskeleton system. D.) The resulting closed loop system has only two inputs. E.) The interconnection of the closed loop amplification exoskeleton with a human stiffness (human compliance $H(s)$). F.) The resulting one-input block diagram. G.) An equivalent representation as the parallel interconnection of two compliances: $C_E(s)$—the compliance of the exoskeleton with respect to external forces, and $\alpha^{-1}H(s)$—the compliance of the human reflected through the amplification effect (amplification rate $\alpha(s)$). H.) A Bode plot of the open loop system, showing mass-like behavior for the exoskeleton, and some phase lag from time delay and low-level control for the actuator-side compliance. I.) A Bode plot of the controller itself. $K(s)$ is designed as $\alpha(s) - 1$ for some desired $\alpha(s)$. J.) A bode plot of the closed loop behavior of the amplification exoskeleton, with the human compliance, $H(s)$, for reference. The human compliance is significant when tuning $\alpha(s)$. K.) Amplification alters the human behavior as it appears for the environment, making the human stronger but altering the phase. The resulting behavior is not necessarily passive, as shown by its phase.

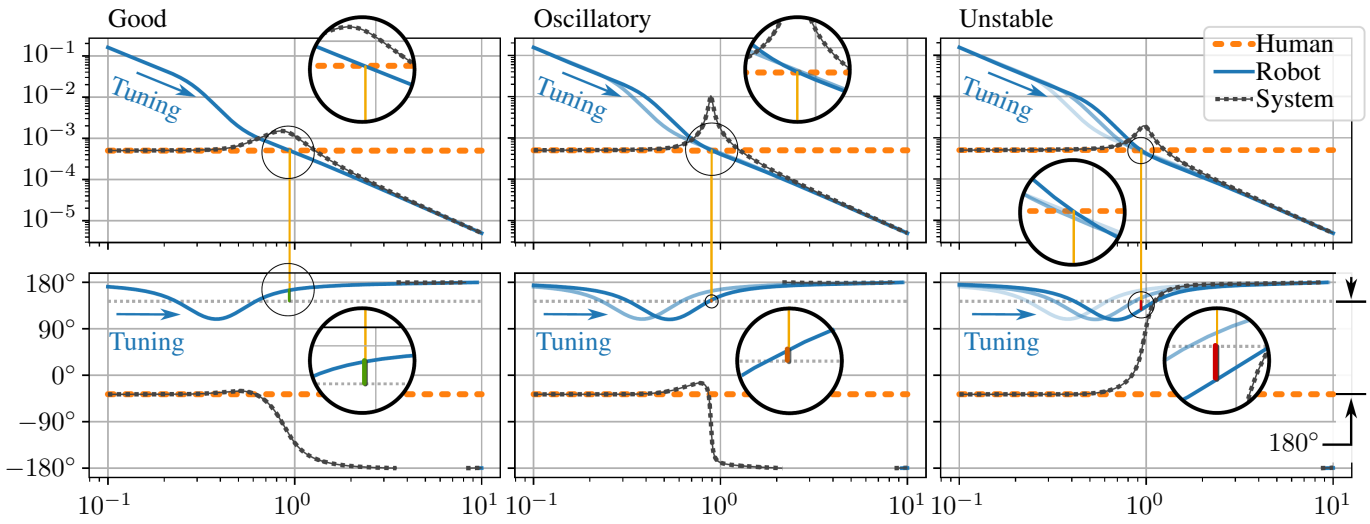

Fig. 3. One parameter tuning of the amplification filter. Three bode plots show three different tuning configurations as the single tuning parameter (the amplification bandwidth) is increased to failure. Plotted are the compliance of the human operator (Human), the compliance of the robot's operator interface (Robot), and the compliance of the two when interconnected in parallel (System). In all three bode plots, magnification is used to highlight the calculation of the "Human Spring Phase Margin." This calculation uses the phase of (Robot) at the frequency where the magnitude of (Robot) is equal to the magnitude of (Human)—the crossover frequency. At this frequency, stability of the resulting human–robot interconnection is determined by comparing the phase of (Robot) to a reference phase 180° offset from the phase of (Human). The difference between the phase of (Robot) and this reference is the "Human Spring Phase Margin."

are stable in interconnection with this human model.

This human phase lag is an imminently exploitable phenomenon in amplification controller design, as the 'Human Phase Margin' criterion is easier to satisfy than the normal one. Our controller exploits this assumption by having an operator-side compliance that asymptotically approaches $-180°$ from below—which would be destabilized by all sufficiently stiff springs. But for humans that follow this model, we can find a minimum stiffness for which all stiffer human behaviors are stable.

This also explains our omission of inertia from the human model. This inertia would also drop the human compliance phase, and would improve the human phase margin (mostly at higher frequencies than our controller operates in practice). Thus, ignoring it doesn't hurt us—it just makes the stability condition more conservative, particularly at high frequencies.

B. Compliance Shaping for Strength Amplification

Fig. 2 shows a progression of block diagrams and four Bode plots which describe the frequency domain model of the system as well as the construction of the controller.

Fig. 2.A shows the one-dimensional representative time domain free body diagram, where the exoskeleton acts like an inertia, and is being acted upon by three forces: the human $f_H(t)$, the actuator $f_A(t)$, and the environment $f_E(t)$. We could describe it,

$$M\ddot{x}(t) = f_E(t) + f_H(t) + f_A(t), \tag{6}$$

where M is the mass of the exoskeleton and $x(t)$ is its position.

We then take this into the frequency domain with Fig. 2.B, where the Laplace transform of the exoskeleton's position, $X(s)$, is the sum of three inputs ($F_E(s)$, $F_H(s)$, and $F_A(s)$ being the Laplace transforms of the environmental force, the human force, and the actuator force respectively) weighted by compliance transfer functions. The compliance of the exoskeleton, $C_E(s)$ is simply the compliance of the exoskeleton inertia:

$$C_E(s) = \frac{1}{Ms^2}. \tag{7}$$

The compliance with respect to actuation forces, $C_A(s)$, introduces some imperfections in control authority. We write these as

$$C_A(s) = C_E(s)\eta(s), \tag{8}$$

and the imperfections in $\eta(s)$ include a low pass filter restricting the bandwidth of the actuation, and a time delay. (A comparison between $C_E(s)$ and $C_A(s)$ is shown in the Bode plot of Fig. 2.H.)

The next block diagram (Fig. 2.C) introduces the controller as a transfer function $K(s)$. This ultimately produces a new human-side compliance $C_H(s)$, as shown in Fig. 2.D. Our controller structures $K(s)$ according to a desired closed loop amplification behavior $\hat{\alpha}(s)$ (not to be confused with the realized amplification behavior $\alpha(s)$). We define the realized amplification as

$$\alpha(s) = \frac{C_H(s)}{C_E(s)} = 1 + \eta(s)K(s), \tag{9}$$

and the desired amplification, $\hat{\alpha}(s)$, is an approximation of this value that neglects the controller imperfections represented in $\eta(s)$, that is

$$\hat{\alpha}(s) = \frac{C_E(s) + K(s)C_E(s)}{C_E(s)} \tag{10}$$

$$= 1 + K(s). \tag{11}$$

C. Second Order Lag Amplification Shape

We parameterize this desired amplification transfer function as a second order lag, with two conjugate poles at lower frequency than two conjugate zeros.

$$\hat{\alpha}(s) = \frac{s^2 + 2\zeta\omega_z s + \omega_z^2}{s^2 + 2\zeta\omega_p s + \omega_p^2}, \tag{12}$$

using the same ζ twice for convenience, though this could potentially be optimized. While this $\hat{\alpha}(s)$ is not strictly causal, it produces a $K(s)$ which is:

$$K(s) = \hat{\alpha}(s) - 1 = \frac{2\zeta(\omega_z - \omega_p)s + \omega_z^2 - \omega_p^2}{s^2 + 2\zeta\omega_p s + \omega_p^2}. \tag{13}$$

This controller is compared to an example of realized $\alpha(s)$ in Fig. 2.I's Bode plot.

The realized behavior can be understood from the Bode plot in Fig. 2.J, which compares the environment side compliance $C_E(s)$ with the human side compliance $C_H(s)$. The human-side compliance has been increased at low frequencies to reach an asymptotic magnification of the environment-side compliance at low frequencies. Also plotted is a representative human compliance, $H(s)$. Following the work of [38], this is modelled as a complex stiffness. That is, the human behaves like a spring with a constant phase lag at all frequencies[2] (suspected to be from hysteretic joint friction). Stability of the human-side compliance when coupled to this human compliance is the key limiting factor on the amplification bandwidth. This will be discussed more with Fig. 3.

D. The Environmental Port

A human compliance in parallel with the closed loop exoskeleton produces a feedback system shown in Fig. 2.E. Closing this loop produces a single input transfer function representing the only remaining input, the environmental force $F_E(s)$, determining the position $X(s)$:

$$\frac{X(s)}{F_E(s)} = \frac{1}{C_E^{-1}(s) + \frac{C_H(s)}{C_E(s)} H^{-1}(s)}, \tag{14}$$

which we write here as a harmonic sum of the two compliances $C_E(s)$ and $\alpha^{-1}(s)H(s)$. This harmonic sum construction can be visualized as these two compliances being interconnected in parallel, as shown in Fig. 2.G.

These two compliances, as well as the total compliance of $X(s)/F_E(s)$ are shown in Fig. 2.K. They illustrate that the application of the inverse amplification rate to the spring-like human compliance reflects it to the environment in a way that is not passive, as we can observe using its phase. This non-passivity is restricted to the mass-type, and the system is potentially destabilized if the human in the exoskeleton tries to move objects that are slightly more massive than the exoskeleton itself (such that the Bode magnitude plot of the offending inertia intersects the total compliance at a frequency corresponding to a non-passive phase). In terms of interacting with spring-like environments, however, the system should work well—and this includes such high-stiffness environments as the ground.

It seems possible that this non-passivity could be avoided if the bandwidth of the amplification were much higher, as in this case the inertia of the exoskeleton could "hide" the non-passivity of the reflected operator. This is hard to do, unfortunately, since the poles of $\hat{\alpha}(s)$ would need to occur at a frequency higher than that of the Bode magnitude plot intersection of $H(s)$ and $C_E(s)$. This brings us to an important point about the minimum-phase property of the zeros of $\alpha(s)$: these zeros are only minimum phase so long as the phase of $K(s)\eta(s)$ at the point where it's magnitude equals unity has not dipped below $-180°$. The phase lag of $\eta(s)$ only drops with frequency, so this acts as a limit on the amplification's bandwidth. To go beyond the natural man-machine resonance would require carefully designed high bandwidth actuation, or operators acting uncharacteristically softly, even when surprised—which seems counter to their instincts. Bandwidth limits and operator safety concerns kept us from attempting this type of control on the real robot.

E. One Parameter Tuning Strategy

Accepting this non-passivity, what remains is to tune the controller to drop the amplification magnitude to the left of the $C_E(s)$–$H(s)$ crossover without making the human–robot system unstable. To facilitate easy tuning of our controller we introduce one parameter λ (equal to ω_p which we tune, and a low frequency amplification gain $\alpha_0 \geq 1$ (equal to ω_z^2/ω_p^2), so that

$$K(s) = \frac{2\zeta(\sqrt{\alpha_0} - 1)\lambda s + (\alpha_0 - 1)\lambda^2}{s^2 + 2\zeta\lambda s + \lambda^2}. \tag{15}$$

Our controller can be tuned without knowing the exoskeleton inertia, human stiffness, or even the human phase lag since λ is the only tuning parameter, the system is stable for infinitesimal λ and the human phase margin decreases as λ increases.

Fig. 3 marks the point at which the total human-side compliance of the exoskeleton intersects a human compliance in the Bode magnitude plot as the crossover point. This frequency of intersection is the human crossover frequency, and the phase of the human-side compliance of the exoskeleton is compared to $-180° - \phi_H$, where $\phi_H > 0$ is the phase lag of the human's stiffness. This "human spring phase margin" determines whether the closed loop system will have a pole in the right half plane, as can be observed from its phase behavior in the Bode plot in Fig. 3. With higher pole frequencies the pole-pair's phase transition becomes more and more abrupt (like that of a perfect oscillator) and eventually becomes unstable—the increasing phase with frequency being a tell-tale indicator of a right half plane pole-pair.

We only need one tuning experiment per degree of freedom to find the limit for any particular amplification shape. Starting with λ very low, we slowly scale it up until the system appears to vibrate. Once the threshold of oscillation is found, the oscillation frequency is roughly the crossover frequency, and we could obtain an estimate of the human phase if we had a good model of the torque tracking performance and time delay. The problem is practically solved, however, by the formulation

[2]For all frequencies below the human's own natural frequency, which is much higher than that of the exoskeleton for our purposes.

of the controller in a one-parameter tunable way. With one knob, it is easy to increase the performance up to the limit, back off for robustness, and get a good result in the end.

F. As a Whole Body Control Task

In this way, we can easily define amplification tasks. For the i^{th} amplification task, we can write the desired task force $f^d_{a,i}$ according to the a (cuff) sensor force in that task dimension $f_{c,i}$,

$$f^d_{a,i}(s) = K_i(s) f_{c,i}(s), \tag{16}$$

where $K_i(s)$ is potentially different for each independent amplification task. In the common case of a six-axis force/torque interface between human and robot, each axis (in some consistent frame) can be amplified separately. As it appears later in our whole body controller, we combine all the amplification tasks together into a big vector

$$f^d_a(s) = \mathbf{K}(s) f_c(s), \tag{17}$$

where $\mathbf{K}(s)$ is a diagonal matrix of all the amplification filters, $f_c(s)$ is a vector of cuff force sensors for each task, and $f^d_a(s)$ is the vector of desired task forces. This last vector is the output of the amplification filtering module, and is treated as the time-domain vector signal $f^d_a(t)$ in Sec. V.

IV. Inter-Foot Force Task

TABLE III
Nomenclature for Sec. IV

Symbol	Meaning
f_i	foot i's spatial force vector in frame $i \in \{1,2\}$
f	stacking of f_1 and f_2
f_s	sum of foot spatial force vectors in frame s
Q_1, Q_2, Q	reaction force cost definition matrices
${}^bX^*_a$	spatial force vector transform, frame $a \rightarrow$ frame b
λ	Lagrange multiplier vector in optimization
X	equality constraint matrix in optimization
Γ	$= [XQ^{-1}X^T]^{-1}$
$\bar{X}$	$= Q^{-1}X^T\Gamma$, a pseudo-inverse of X
f_d	inter-foot force task error in frame d
$\tilde{X}$	weighted inter-foot difference matrix
$\mathbf{G}$	virtual base definition matrix

Human-led contact transitions are an important part of any scheme for controlling multi-contact exoskeletons, and they do not fall out of the strategy for strength amplification naturally. To allow this critical feature we introduce a second task which, if satisfied, causes the robot to lift the foot when the human does.

Strength amplification for multi-contact robots can be thought of as a reduction to fixed based dynamics plus an application of the fixed base solution. However the virtual "base" can change with time. When two feet are on the ground at the same time, we can imagine a virtual single foot between them which acts like a base. In this case the internal forces between the two feet can also be controlled, and this internal force degree of freedom can be thought of as a part of the corresponding fixed base model's environmental force reflection problem. Additionally, unlike an actual fixed base robot, multi-contact robots can topple over. An exoskeleton is essentially a humanoid robot in multi-contact with a human, and the inequality-constrained floating base models [44], [45], [46] are still relevant to keeping its feet from tipping or slipping. To avoid tilting or sliding the contacts, additional inequality constraints must be maintained—and the variables that define these base–ground forces are not part of a standard fixed base robot model, but are expressed as the Lagrange multipliers of the contact constraint that defines the virtual base.

The goal of our exoskeleton in multi-contact is to accomplish the desired tasks. And this is accomplished by allowing the force at the "base" to be whatever necessary to accomplish the other objectives, within their constraint limits. When these constraint limits are hit, it is assumed that something will have to be sacrificed.

We define a virtual base for the robot by defining the way that virtual base would distribute forces between the two feet. We consider the following equality constrained quatratic programming problem which optimally distributes the net reaction forces between two feet.

$$\underset{f_1,\ f_2}{\text{minimize}} \quad \frac{f_1^T Q_1 f_1}{2} + \frac{f_2^T Q_2 f_2}{2} \tag{18}$$

$$\text{subject to} \quad {}^sX_1^* f_1 + {}^sX_2^* f_2 = f_s, \tag{19}$$

where Q_1 and Q_2 are positive definite and typically diagonal, ${}^sX_1^*$ is the transform between representation in the foot1 frame and some new "sum" frame for spatial force vectors, and ${}^sX_2^*$ is the same for the other foot, and f_s represents the net force in "sum" frame.

This type of problem can be solved with matrix inversion:

$$\underbrace{\begin{pmatrix} Q_1 & \\ & Q_2 \end{pmatrix}}_{Q} \underbrace{\begin{pmatrix} f_1 \\ f_2 \end{pmatrix}}_{f} + \underbrace{\begin{pmatrix} {}^sX_1^* & {}^sX_2^* \end{pmatrix}}_{X}{}^T \lambda = 0, \tag{20}$$

$$Xf = f_s. \tag{21}$$

In matrix form,

$$\begin{pmatrix} Q & X^T \\ X & 0 \end{pmatrix} \begin{pmatrix} f \\ \lambda \end{pmatrix} = \begin{pmatrix} 0 \\ f_s \end{pmatrix}, \tag{22}$$

$$\begin{pmatrix} f \\ \lambda \end{pmatrix} = \begin{pmatrix} Q^{-1} - \bar{X}XQ^{-1} & \bar{X} \\ \bar{X}^T & -\Gamma \end{pmatrix} \begin{pmatrix} 0 \\ f_s \end{pmatrix}, \tag{23}$$

where $\Gamma = [XQ^{-1}X^T]^{-1}$ and $\bar{X} = Q^{-1}X^T\Gamma$. Thus

$$f = Q^{-1}X^T[XQ^{-1}X^T]^{-1} f_s, \tag{24}$$

$$\begin{pmatrix} f_1 \\ f_2 \end{pmatrix} = \begin{pmatrix} Q_1^{-1}{}^sX_1^{*T} \\ Q_2^{-1}{}^sX_2^{*T} \end{pmatrix} \cdot \left({}^sX_1^* Q_1^{-1}\, {}^sX_1^{*T} + {}^sX_2^* Q_2^{-1}\, {}^sX_2^{*T}\right)^{-1} f_s \tag{25}$$

With this solution defining the virtual base, or desired force distribution, we go on to parameterize the other six degrees of freedom in the foot forces—the difference from the desired distribution. This difference force vector is defined using its influence on the two foot forces

$$f = \bar{X} f_s + \left[I - \bar{X}(\bar{X}^T\bar{X})^{-1}\bar{X}^T\right] \tilde{X}^T f_d \tag{26}$$

where we introduce

$$\tilde{X} = \begin{pmatrix} {}^dX_1^{-*} w_2 \\ -{}^dX_2^{-*} w_1 \end{pmatrix}, \tag{27}$$

as a rough parameterization of the deviation from the desired force distribution. This gets contorted into being perpendicular to $\bar{X}$ by the pre-multiplication with a $\bar{X}$ image space nullifier. Ultimately we make reducing $\|f_d\|$ a task, and when it is satisfied the reaction forces minimize the previously defined quadratic cost (since $f = \bar{X} f_s$). This leaves f_s as the path of least resistance the optimization uses to hold up the weight of the robot.

We define $\mathbf{G}$ to simplify this equation:

$$f = \mathbf{G} \cdot \begin{pmatrix} f_s \\ f_d \end{pmatrix}, \tag{28}$$

$$\mathbf{G} = \begin{pmatrix} \bar{X} & \left[I - \bar{X}(\bar{X}^T \bar{X})^{-1} \bar{X}^T\right] \tilde{X}^T \end{pmatrix}. \tag{29}$$

Our exoskeleton controller is tasked with simultaneously accomplishing amplification at the hip (Sec. III) and a zeroing of this new variable f_d, which we call the "difference task". The hip sensor force task serves a similar purpose to the centroidal momentum tasks introduced in [44] or the COM task in [47], as it relates the total force on the body to the required reaction forces. This hip zeroing task is directly influenced only by the sum of reaction forces. Ultimately we also describe these reaction forces as a function of the joint torques, but we can also think of this hip task as determining the sum of the reaction forces. Clearly, the difference task (itself similar to a CoP task from [47]) determines part of the reaction force vector too. With both tasks active, the reaction forces are all defined and the joint torques can be thought of as resulting from an inverse dynamics process—as in the Dynamic Balance Force Control of [48].

V. Weighted 1-Norm Shared Body Control

TABLE IV
Nomenclature for Sec. V

Symbol	Meaning
τ	optimization variable: joint torque vector
M_e, B_e, g_e	exoskeleton mass, Coriolis, gravity
$\ddot{q}$, $\dot{q}$, q	joint acceleration, velocity, position
S	underactuation matrix for a free floating base
J_c, f_c	Jacobian for human contact and forces
J_r, f_r	Jacobian for ground contact and (reaction) forces
C_r, c_r	foot contact inequality matrix and bias
$e(\cdot)$	a task error function
$\sigma(\cdot)$	a task scalarization function
s_+, s_-	1-norm slack variables
w	weight vector
J_a, f_a, $\ddot{x}_a$	Jacobian, force, accel. for all amplification tasks
J_f, f_f, $\ddot{x}_f$	Jacobian, force, accel. for feet
$\mathbf{J}$, $\mathbf{f}$, $\ddot{\mathbf{x}}$	Jacobian, force, accel. for composite task
$\bar{\mathbf{J}}$	Dynamically consistent pseudo-inverse of $\mathbf{J}$
Λ	inertia matrix in composite task frame
$\mathbf{G}$	virtual base definition matrix
$\bar{\tau}$	maximum torque, human + exoskeleton
f_a^d	vector of desired amplification task forces

The basic dynamics of an exoskeleton in (multi-)contact with the ground can be written in the notation of Tab. IV as

$$M_e \ddot{q} + B_e + g_e = S\tau + J_c^T f_c + J_r^T f_r, \tag{30}$$

$$J_r \ddot{q} + \dot{J}_r \dot{q} = 0, \tag{31}$$

where these equations only hold as long as,

$$C_r f_r + c_r \geq 0. \tag{32}$$

That is to say, so long as the feet do not slip or pull up on the ground. In addition to these limits due to contact, there are upper bounds to the torque magnitude the robot can provide. And if some of the joints are not actuated, then they have an upper limit of zero. These inequalities, when active, prevent the simultaneous satisfaction of all the robot's goals. This presents a clear problem for the whole body controller: how should the robot behave when the inequalities constrain the robot's ability to satisfy its tasks?

Our approach to this problem is to prioritize the tasks. And then, because a strict prioritization is not computationally feasible for our hardware, we approximate the lexicographic optimization with a 1-norm cost. Additionally, we reduce the size of the optimization problem by representing all reaction forces in terms of joint torque.

A. Prioritized Tasks

With multiple tasks and inequality constraints, the robot's behavior is often over-specified. For example, the following two tasks and set of inequality constraints can (and often do) conflict: the task to apply zero lateral (y-axis) hip force to the human, the task to apply zero roll rotation (x-axis) about the hip, and the inequality task to maintain forces within the friction cones of the two feet cannot be simultaneously satisfied when the center of mass is not above the support region of the contact state [49]. This happens frequently during dynamic walking. And it demands that we specify not only which tasks we want to achieve, but in which order they should fail to be satisfied if they conflict in this way.[3]

Without an analytical method to determine the relative desirability of the various solutions to the over-constraint problem, we must rely on our intuition and trial and error. One method that lends itself to this informal design process is the prioritization of the tasks relative to eachother. This approach has also been used to handle redundancy in task definition even without the limitation of constraints[47]. Using priorities we simply specify which tasks we want to "survive the longest" when the inequality constraints cause fewer and fewer tasks to be accomplished. The lowest priority tasks are the ones for which we feel the human will have the easiest time comfortably handling the task failure. In the case of our amplification tasks, this could mean both a failure to amplify the interaction force or a failure to achieve gravity compensation. In the case of our inter-foot force task it could mean applying a force to the user's swing foot (failure to gravity compensate) or failing to match the user's desired contact force distribution (failure to transition appropriately, most evident if a foot is load bearing when it should not be).

Strict prioritization between the tasks is a mathematically well defined optimization scheme known as lexicographic

[3]After trying both prioritizations, we determined that the operator prefers a failure in x-axis torque balance, even if this causes the exoskeleton's hip to "wobble" relative to the human's with every step due to the compliance of the backpack attachement in this degree of freedom.

optimization [50]. However, to solve a lexicographic problem entails great computational work. Linear lexicographic costs with linear constraints and inequalities require solving one linear programming problem for each level of cost hierarchy. In our hardware, we could solve a linear program of roughly equivalent size only three times per time-step, so with 12 tasks this was outside the realm of plausibility.

B. Weighted 1-Norm Cost

Ref. [50] shows that weighted scalarization costs can approximate a lexicographic optimization in the context of humanoid control. We used a scalarization which retains the linearity of the cost function, but we added two positive slack variables and two inequality constraints for each scalarized cost (which were all task elements) in order to do so. For our vector of task errors $e(\tau)$ (expressed as a function of torque, as will be elaborated on in Sec. V-C), we define a vector of scalarizations $\sigma(\tau)$

$$\sigma(\tau) = s_+ + s_- \tag{33}$$

where

$$s_+ \geq e(\tau), \qquad \text{and} \qquad s_- \geq -e(\tau), \tag{34}$$

where s_+, and s_- are the newly introduced vector slack variables, and the new vector inequalities in (34) are elementwise inequalities. Under conditions which are almost always met[4], $\sigma(\tau) = |e(\tau)|$ (as an elementwise absolute value).

This approach to modelling an absolute value function within the confines of a linear programming problem is the key to our application of a weighted 1-norm cost on the vector of all task errors. Clearly, summing the elements of $\sigma(\tau)$ results in the vector 1-norm of $e(\tau)$. Summing the elements of $\sigma(\tau)$ with positive weightings (setting cost equal to $w^T\sigma(\tau)$ for some vector of positive weights w) is a weighted scalaraization in the sense of [50], but we can also think of it as a weighted 1-norm—as the 1-norm for a scaled version of the original space. We prefer this as a name for the way it invokes a lozenge-like rhomboid geometry in 2D, and a diagonally-scaled octahedron geometry in 3D.

To solve a lexicographic problem accurately requires iteration, with the first problem optimizing over the highest priority task, and subsequent tasks operating with the solution prior problems acting as constraints. Each sub-problem in the lexicographic solution is slightly smaller than the approximation we propose, but our problem requires only one linear program to be solved, and only adds twice as many variables and inequalities as the number of cost elements in the first lexicographic sub problem. Our approach was able to reliably solve within our single millisecond real-time controller window.

To capitalize on this 2D intuition, Fig. 4 illustrates how the weighted 1-norm cost can be adjusted through the weighting to approximate different lexicographic costs (there are only two in 2D space). The illustration features a convex 2D set of solutions which satisfy constraints. The two axes represent orthogonal tasks, with the origin representing perfect satisfaction of both tasks. Cost A uses a weighting that penalizes the vertical error more than the horizontal, while cost B penalizes them roughly equally. In both cases, the minimum cost point which satisfies constraints is highlighted, and is to be on one of the two axes. The lexicographic optimum for a cost that prioritizes horizontal error infinitely over vertical error coincides with the optimal solution for cost B, and the same is true of the opposite lexicographic ordering and cost A. The fact that these 1-norm costs can be exploited to produce "sparse" solutions (solution vectors containing many zeros) is frequently exploited [51]. The 1-norm does not guarantee sparsity, but is merely "sparsity-promoting". In our illustration, sparsity occurs because the weightings in A and C are more extreme than the slope of the relevant constraint inequalities. Cost B illustrates the non-sparse case, where a vertex of the valid space is optimal due to insufficiently biased task weighting.

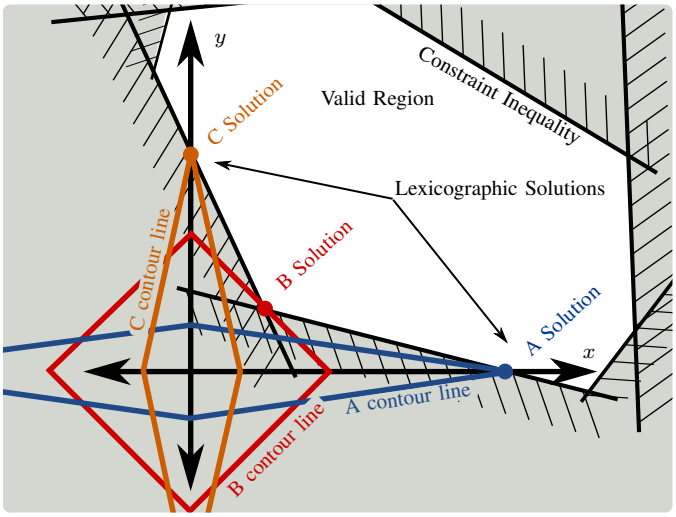

Fig. 4. Illustration of how weighted 1-norm costs can behave similarly to lexicographic (prioritized) costs. Plot in the space of task error for task-x and task-y. Weighted 1-norm costs A, B, and C are depicted with a single contour line each. Optimal solutions for each task shown as colored circles. The so-called "sparsity promoting" nature of the weighted 1-norm cost can be understood in this context as optimal solutions which sacrifice one task to achieve the other. As exemplified by cost B, however, this is not guaranteed and depends on the inequality constraints and the shape of the valid region they generate.

One disadvantage of weighted 1-norm costs in robot control is that the constraints are continuously varying due to the changing robot geometry, and this can cause the optimal behavior to jump discontinuously. This can occur if the 1-norm cost discontinuously switches from being aligned with one lexicographic solution to a different lexicographic solution or even a non-lexicographic solution. We call this a priority inversion event, and one of our goals in setting up the prioritization is to minimize the chance that they occur. For this reason we can think of the 1-norm cost as having lost something important in exchange for its speed. Fortunately, the approximation of the lexicographic problem is asymptotically perfect as the weight discrepancy increases, and the numerical

[4]Specifically that each element of $\sigma(\tau)$ appears in the cost with a strictly positive weight, and that $\sigma(\tau)$, s_-, and s_+ are otherwise decoupled from the problem.

precision of the linear program solver allowed us sufficient space to set these weights orders of magnitude apart and achieve reliable reproduction of the lexicographic problem in practice.

C. Actuator-Mapped Reaction Force Space

In order to speed up the solver and increase its accuracy, we reduce the number of free variables in our optimization problem by handling some equality constraints in advance. This is not necessary theoretically, as the problem is not actually changed by handling these constraints, however attempts to lean on the solver's own ability to perform linear algebra resulted in disappointing precision and speed. Thus we found the need to quickly re-express reaction forces as functions of joint torque.

In addition to being constrained by ground contact, a multi-contact exoskeleton is constrained to follow the position of the human at certain attachment points. In addition to a connection at both feet, our exoskeleton has an attachment at the backpack, for example. While it is possible to imagine advanced exoskeletons which have more degrees of freedom than are constrained by the attachment to the human, we have not deeply investigated this case. Here, we consider the total constraint between the exoskeleton and its environment, which includes both the ground and the human operator, as the combination of the degrees of freedom from all the various amplification tasks (those represented in J_a, f_a, and $\ddot{x}_a$) and the feet degrees of freedom (J_f, f_f, and $\ddot{x}_f$ which are the same as J_r, f_r, $\ddot{x}_r = 0$ in dual support, but still include both feet in single support), such that a new composite Jacobian, $\mathbf{J}$, force vector, $\mathbf{f}$, and task acceleration, $\ddot{\mathbf{x}}$ can be defined:

$$\mathbf{J} = \begin{pmatrix} J_a \\ J_f \end{pmatrix}, \qquad \mathbf{f} = \begin{pmatrix} f_a \\ f_f \end{pmatrix}, \qquad \ddot{\mathbf{x}} = \begin{pmatrix} \ddot{x}_a \\ \ddot{x}_f \end{pmatrix}. \tag{35}$$

Beginning with the physical equations, we can reformat the dynamics of the robot as a matrix equality with an analytic solution,

$$\begin{pmatrix} M_e & \mathbf{J}^T \\ \mathbf{J} & 0 \end{pmatrix} \begin{pmatrix} \ddot{q} \\ -\mathbf{f} \end{pmatrix} = \begin{pmatrix} -B_e - g_e \\ \ddot{\mathbf{x}} - \dot{\mathbf{J}}\dot{q} \end{pmatrix} + \begin{pmatrix} S \\ 0 \end{pmatrix} \tau, \tag{36}$$

which can be solved as in (23). The S matrix represents the under-actuation due to the floating base (under-actuation due to non-actuated mechanical joints is handled separately, through joint torque limits). We define the dynamically consistent pseudo inverse of $\mathbf{J}^T$, $\bar{\mathbf{J}}^T$, satisfying $\bar{\mathbf{J}}^T\mathbf{J}^T = I$ (a left inverse), but likely *not* satisfying $\mathbf{J}^T\bar{\mathbf{J}}^T = I$:

$$\bar{\mathbf{J}}^T = (\mathbf{J}M_e^{-1}\mathbf{J}^T)^{-1}\mathbf{J}M_e^{-1}. \tag{37}$$

And we define inertia in the composite task frame $\Lambda = (\mathbf{J}M_e^{-1}\mathbf{J}^T)^{-1}$. Together, these allow us to state the result,

$$\mathbf{f} = \Lambda\ddot{\mathbf{x}} - \Lambda\dot{\mathbf{J}}\dot{q} + \bar{\mathbf{J}}^T(B_e + g_e) - \bar{\mathbf{J}}^T S\tau. \tag{38}$$

Some terms in the previous expression are more significant than others, and some of the less significant terms are also corrupted by both imperfect knowledge of the robot's mass matrix and (filtered) differentiation noise inherent in using quantized position sensors to estimate velocity and acceleration estimates. We did not notice a significant drawback in switching to a simplified version which represents a steady state equilibrium:

$$\mathbf{f} = \bar{\mathbf{J}}^T(g_e - S\tau). \tag{39}$$

Of course, if we moved fast enough, these ommisions would be noticable. With this simplification, swinging the swing foot very fast should require the operator to resist the centrifical extension of the knee due to the inertia of the exoskeleton. Also, squatting very quickly should result in a non-zero backpack sensor force due to the neglected acceleration terms. However, at the speeds we tested these effects were dwarfed by other control and mechanical imperfections. We hope that future exoskeletons will achieve such mastery over the basic terms that these dynamic terms will regain relevancy.

D. A Linear Program for Shared Body Control

The passive joints make it impossible to achieve all the objectives, and when the robot reaches the limits of its ground contact support, this further restricts the objectives—forcing the sacrifice of another degree of freedom. We approach this problem by attempting to prioritize the various degrees of freedom in the force matching goal of the exoskeleton so that when the constraints come into play, the resulting behavior is predictable and the most important goals are sacrificed last.

$$\begin{aligned}
\underset{\tau, s_+, s_-}{\text{minimize}} \quad & w^T s_+ + w^T s_- && \text{(40a)}\\
\text{subject to} \quad & C_r f_r(\tau) + c_1 \geq 0, && \text{(40b)}\\
& \tau \leq \bar{\tau}, \qquad -\tau \leq \bar{\tau}, && \text{(40c)}\\
& s_+ \geq e(\tau), \qquad s_+ \geq 0, && \text{(40d)}\\
& s_- \geq -e(\tau), \qquad s_- \geq 0, && \text{(40e)}
\end{aligned}$$

where $f_r(\tau)$ and $e(\tau)$ are linear functions of τ. These functions are based on (38) or (39), which define $\mathbf{f}(\tau)$, (35) which splits $\mathbf{f}(\tau)$ into $f_f(\tau)$ and $f_a(\tau)$ parts,

$$\begin{pmatrix} f_s(\tau) \\ f_d(\tau) \end{pmatrix} = \mathbf{G}^{-1} f_f(\tau), \tag{41}$$

$f_r(\tau)$ being some part of $f_f(\tau)$ according to stance, and

$$e(\tau) = \begin{pmatrix} f_d(\tau) \\ f_a(\tau) - f_a^d \end{pmatrix}, \tag{42}$$

recalling the matrix $\mathbf{G}$ from the definition of the inter-foot task in Sec. IV and the vector f_a^d from the definition of the amplification task in Sec. III.

We call this program "Shared Body Control" because the human and the robot's torque and contact forces are both relevant. The true conditions for tipping over the foot are a function of both human and exoskeleton reaction forces. The sum of the human and robot reaction forces needs to lie within the friction cone, but sometimes the human works to counterbalance large torques the robot applies to the ground. We cannot know the human forces given our sensor configuration, so we are forced to be either optimistic (risking failure) or very conservative. Taking the conservative route means that our constraint will occasionally interfere with our tasks unnecessarily.

The human is also the only possible source of torques for the passive joints. By relaxing the torque requirements on the passive joints, the optimization will produce a torque vector representing a sum of exoskeleton and human originated torques. While we cannot expect the human to implement such torques, we can use this technique to prevent the exoskeleton from abandoning tasks which it could accomplish with help from the human (bounded, of course, by $\bar{\tau}$).

VI. Implementation in Hardware

To better understand the behavior of this complex control strategy, we turn to the behavior of a physical realization in a lower body exoskeleton.

A. Hardware

Our hardware platform is the Sagittarius P5 lower-body exoskeleton from Apptronik Systems, shown in Fig. 1. This exoskeleton has 12 joints, six per leg. We name the joints in the serial kinematic chain from the torso to the foot 1) hip abduction/adduction, 2) hip flexion/extension, 3) hip internal/external rotation (hip yaw), 4) knee flexion/extension, 5) ankle flexion/extension, and 6) ankle pronation/supination (ankle roll). Of these six, four are powered joints. The two passive joints are hip internal/external rotation (also referred to as hip yaw for alignment with the local z axis) and ankle pronation/supenation (which we also call ankle roll for similar reasons). The powered hip abduction and hip flexion joints are actuated by rotary series elastic actuators, while the other two feature proprietary linkage designs connecting linear series elastic actuators with rotary joint motion. Power is provided from off-board the device via a joint power and communication tether. The actuators communicate with a realtime Linux desktop workstation through an ethercat bus.

The different parts of the exoskeleton are highlighted in Fig. 1, with rigid bodies being bordered by different color lines on the spectrum from blue to purple, human attachment points in orange, and safety features in red. To ensure the safety of the operator, the exoskeleton is attached via a slack safety rope to an overhead gantry system, and the rope's height is operated by an assistant when the height is changing rapidly (as in the stair-climbing task pictured in Fig. 1. The operator wears a helmet, and there are multiple easy ways to stop the exoskeleton in an emergency: 1) a software emergency stop button, 2) a button on the top of the main back-pack circuitry box, and 3) a button which the operator is required to hold at all times.

B. Controller Implementation

While we have presented the controller design in a very general way, not all of its nuanced behavior is relevant enough to demand implementation in the hardware system we used. In particular, the dynamic terms in (38) were not large enough for the operator to notice their omission, and the dynamically consistent pseudo-inversion of $\mathbf{J}$ is unnecessary given that $\mathbf{J}$ is invertible with the tasks we defined, thus

$$\mathbf{f} = \mathbf{J}^{-T}(g_e - S\tau). \tag{43}$$

Note that when an amplification task has $K(s)$ set to zero, it becomes essentially a gravity compensation task; finding τ such that the appropriate elements of $\mathbf{f}$ are zero being equivalent to finding it such that the equality $g_e = S\tau$ holds for some particular row space.

To summarize the tasks of the controller, the backpack–exoskeleton force/torque sensor value is re-expressed in a hip-center frame, and the six individual Cartesian components are then fed into a diagonal matrix of amplification compensators as described in Sec. III. For the three sagittal plane forces and torques (x-force, z-force, and y-torque) we may apply non-zero amplification, but the other three are left at zero in this work. This is based on the physical intuition that the sagittal plane forces and torque represent the larger interaction quantities during walking. This forms a six-dimensional amplification task. Based on a bed of 12 insole-mounted pressure sensitive resistors, a rough estimate of the human center of pressure is produced. This estimate is used to construct the elements of the inter-foot force task, which is also a 6 dimensional task. With this hardware specific pre-processing completed, the tasks are sent to a separate and more generic module to perform the linear programming optimization work. The software implementation of this optimization process is separate from the Apptronik control framework, and is available as open source software [52]. It primarily acts as a wrapper layer for the linear programming solver from the COIN-OR [53] community.

Fig. 5 describes the sensor configuration on the Sagit exoskeleton and contrasts this to the way we visualize the behavior of the optimization problem. Fig. 5.a shows the HCRL logo wearing the exoskeleton, colored dark gray for the structure of the exoskeleton, yellow for the visible force sensors, and green for the parts of the exoskeleton which are considered to be part of the human (the human attachments). In Fig. 5.b only the exoskeleton and the sensors are displayed, revealing the shoe inserts, with sensorized pads and an additional force sensor on the back. In Fig. 5.c we label the three human attachments as they are numbered in the code. Fig. 5.d introduces the visualization of the optimization configuration, where the operator (without its mass) and the exoskeleton are grounded at attachments which happen to correspond to the human interfaces. With the exoskeleton and massless operator hanging from these grounding points, the job of the exoskeleton is to choose the joint torques which minimize some cost—which essentially identifies two groundings to avoid using (Fig. 5.e). For example, if the steady state amplification rate is non-amplifying, i.e. $\alpha_0 = 1$, then the hip amplification task directly penalizes the 1-norm of forces on ground 0—the fictitious connection between the exoskeleton and the world at the backpack. When the human's weight is on the left foot (interface 1) the foot cost penalizes the 1-norm of ground 2—the right foot's friction grounding, resulting in the robot deciding to support its weight as far as possible from ground 1—the left foot. The significance of the massless operator is that the optimization gives an allowance for the human to help the shared control system exceed the limitations of the robot's own actuators. This means the robot is unlikely to abandon a task simply due to the passive joints,

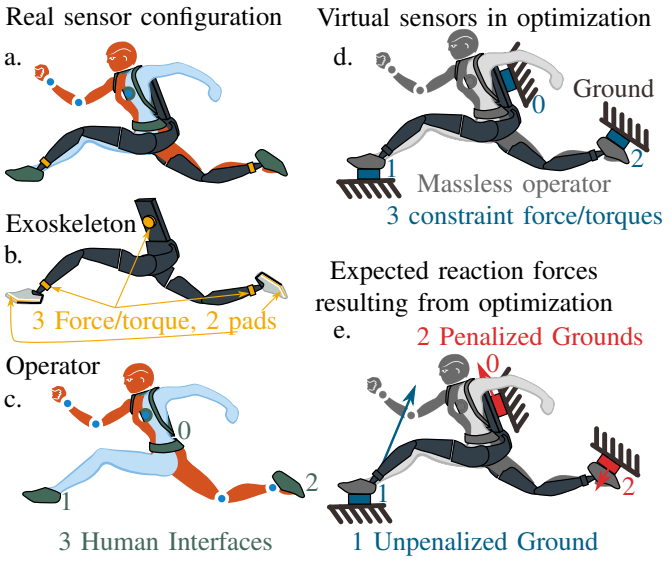

Fig. 5. Sensor configuration, real sensors for strength amplification and virtual sensors used to define the tasks.

but it will if achieving this task would put unreasonably high strain on the human's ankle roll and hip yaw joints.

C. Priorities

One might suspect that the order of task importance would be easy to determine a priori, but it was a rather empirical weighting process in practice. First, seeking to fall back to the linear inverted pendulum behaviors of a point foot robot (that is, prioritizing amplification in the direction between the center of mass and the center of pressure as well as amplification in hip pitch—similar to the hip tasks of the Hume biped [45]) we found them to frustrate the operator with their naturally unstable lateral position. The weightings in Tab. V sacrifice x-torque first, which seems to be more comfortable for the operator. However, this preference may be exoskeleton or operator specific. The main limitation of these parameters is that at each stance transition the hips of the device roll such that the stance hip is higher than the swing hip—likely due to the lower penalty on hip amplification x-torque. However, we must sacrifice something, and this appeared to be the least-uncomfortable choice. The large swing in the hip position is due to the rather loose coupling that the back-pack provides in this degree of freedom.

In testing, we began to suspect that operators may prefer a lower task penalty on the difference task while in double support, but react strongly negatively to difference task violation while in swing (since this entails the exoskeleton loading their swing foot). We made a slight modification to the sum scalarized cost for the difference tasks by implementing a two part cost function: the sum of a one-norm penalty as described before and a second one-norm penalty with a non-zero minimum value or "dead zone" and a higher weighting. In Tab. V these extra additions to the cost weighting are reported as the "Limit Penalty." What this means is that within the dead zone, the cost acts like the original weighted 1-norm cost (plus a constant bias that does not influence the optimum), and at the boundary of the dead zone the weight suddenly becomes much higher. We scheduled the dead zone width based on the center of pressure location, such that in single support this dead zone collapsed to zero and the difference task essentially took on the higher weighting of the limit penalty penalty. In dual support, the width of the dead zone reached its widest when the feet were evenly balanced, and reduced linearly in either direction away from that midpoint.

TABLE V
IMPLEMENTED TASK PRIORITIES

Task	Weighting
Hip Amplification x-Force	1×10^5
Hip Amplification y-Force	1×10^5
Hip Amplification z-Force	1×10^5
Hip Amplification x-Torque	1×10^0
Hip Amplification y-Torque	1×10^1
Hip Amplification z-Torque	1×10^5
Diff Task x-Force, Limit Penalty	1×10^{-1}, 1×10^5
Diff Task y-Force, Limit Penalty	1×10^{-1}, 1×10^5
Diff Task z-Force, Limit Penalty	1×10^{-6}, 1×10^6
Diff Task x-Torque, Limit Penalty	1×10^{-6}, 1×10^5
Diff Task y-Torque, Limit Penalty	1×10^{-6}, 1×10^5
Diff Task z-Torque, Limit Penalty	1×10^0, 1×10^5

TABLE VI
EXPERIMENTAL PARAMETERS

Test	SBC	α_0	Load
VI-D.1	Off	0	0 N
VI-D.2	On	0	0 N
VI-D.3	On	0	110 N
VI-D.4	On	3	110 N

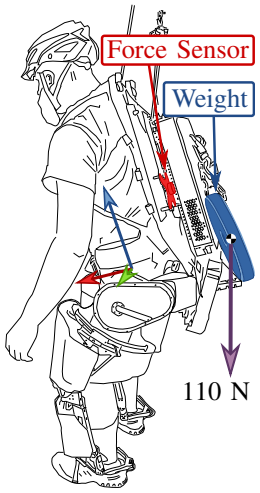

Fig. 6. Load position in VI-D.3 and VI-D.4. Load hangs from a chain attached to the exoskeleton. Human effort measured with a six-axis force torque sensor, highlighted in red. Measurements are presented in the pictured "hip center" coordinate frame.

D. Demonstrating the Amplification Task

We conducted a set of simple tests to demonstrate the difference between gravity compensation and human strength amplification. These tests aimed to demonstrate an improvement in amplification stability relative to previous controllers developed for the exoskeleton and its previous partial prototypes (the 1-DOF testbed from [39], [40], a two degree of freedom leg, and a previous revision on the same lower body design) under the same project [31], which was a condition of our using the exoskeleton[5].

Fig. 6 and Tab. VI show the basic structure of our tests: the operator wears the exoskeleton in a roughly standing position and various controller features are turned on and off. Extra

[5]Which is to say, our testing time was limited, and the scope of our experiments was narrow.

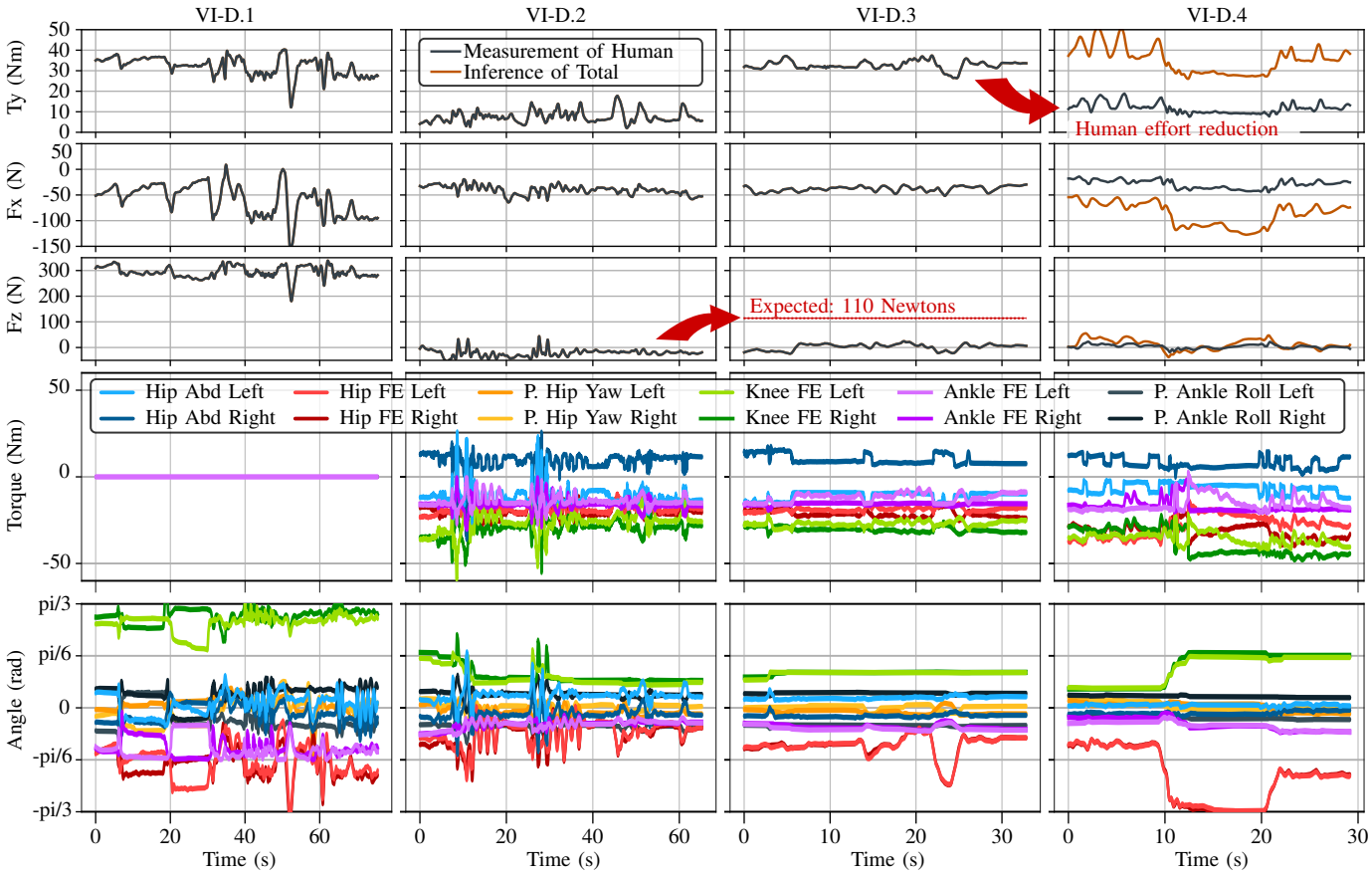

Fig. 7. Four way sagittal hip force comparison (see Sec. VI-E).

weight is attached to the backpack as an unknown load in tests VI-D.3-4, and the image shows where it hangs relative to the operator. Fig. 7 shows the results of the three tests.

E. Discussion of Amplification Task

In the first test, VI-D.1 the exoskeleton joints are on, but the desired torque is zero. The first column of plots in Fig. 7 show the large z-force on the backpack due to the gravitational load of the exoskeleton acting on the operator. Variation in the angle shows that the operator was not perfectly holding still over the duration of the test. This, while it prevents us from easily comparing across experiments (the operator doesn't even have the same resting posture between loading configurations) is hard to compensate for or avoid.

The next test, VI-D.2 enables gravity compensation—which means the torques from the shared body controller are applied to the robot, but the amplification filters are all set to apply no strength amplification feedback ($\alpha_0 = 1$, so $f_a^d = 0$). This drastically reduces, but does not entirely eliminate the interface forces and torques. Even if the robot's mass parameters were perfectly modeled, the operator would still need to apply forces through this interface to control the passive joints of the robot. Compensating for the weight of the heavy exoskeleton is the most significant component of the system's behavior.

In test VI-D.3, we added an 11 Kg (25 lb) mass to the backpack, without changing the control mode. The test does not focus on the transient response, but on the steady state behavior with the weight (mechanically, it would be hard to make the weight addition appear sudden without dropping it). We see some unexpected behavior in the vertical sensor force: the weight's 110 N are not felt. This suggests a "force leak" in the design of the backpack sensor, where the force of the added weight is transferred to the operator without passing through the sensor. A likely culprit is the hip-pad of the backpack (directly connected to the operator) and the hips of the exoskeleton—as this would be consistent with the clear increase in the y-torque.

In the final test, VI-D.4, we engaged the amplification filters—providing a steady state amplification factor of 3, and a zero pair at 1 Hz for all three degrees of freedom in the sagittal plane. By choosing these conservative settings, we were able to both exceed the amplification performance of our previous multi-joint amplification controllers and achieve stability on the first try[6]. As shown in Fig. 7's fourth column, the human's effort was reduced to roughly a third of its value in the third column in the y-torque component. The inference of the total human-and-robot force is shown as well, and should reflect a rough continuation of the value in the previous set of plots. This value is computed based on an internal state value from the frequency domain compensator, and is not "aware" of the

[6]A later gain-tuning experiment revealed that the bandwidth limit is higher than this, but we ran out of time for exhaustive identification of this limit.

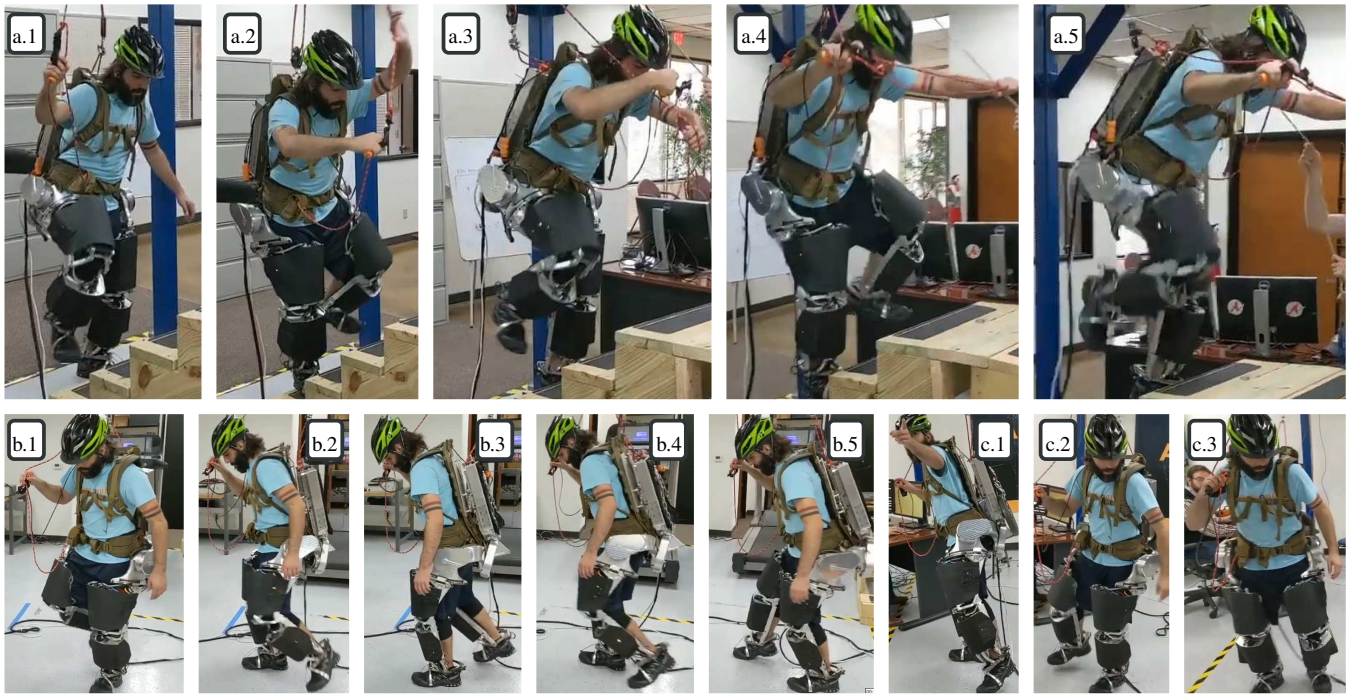

Fig. 8. Frames from the demo. Frames a.1-5: climbing stairs with amplification but no added weight. Frames b.1-5: walking around. Frames c.1-3: walking around with amplification and extra weight.

saturating effects of the inequality constraints in the shared body controller. So it is hard to tell if the changes, in for example the x-force plot, are due to ground contact constraints or the ever-changing stance position of the operator. Despite all these complicating factors, it is clear that engaging the amplification reduced the measurements of the human effort relative to what is was after the attaching of the load.

F. Discussion of Foot Transitions

With or without amplification, the primary behavior of the system was to use shared body control to partially compensate the robot's own gravity while allowing human-led foot transitions through the inter-foot force task. Since the robot itself was based on high bandwidth torque controlled actuation, the operator could easily backdrive it to climb up stairs or to stand on one foot. Since this was the case gravity compensation was the dominant effect of the controller, with amplification acting in a supplemental role. But for both of these behaviors, the control of the contact transitions via the inter-foot force task was key.

Fig. 8 shows the operator shifting weight from one foot to another and lifting up the legs one at a time. Good human-led transitions are the key to this behavior, and are achieved by controlling the weightings Q_1 and Q_2 matrix that determine $\mathbf{G}$ to reduce future-swing-leg reaction force in advance of the foot lifting. When the human shifts weight to one foot, the Q matrix penalty for reaction forces on the other foot becomes much larger. And since this causes the COP of the robot to approximate the COP of the human, this prevents the human from needing to lift a load-bearing robot leg. In addition, the penalty limit method allowed the exoskeleton more freedom during dual support, but smoothly reduced this freedom when approaching single support, so that by the time it was reached the inter-foot force task was essentially the highest priority.

This behavior is shown in more detail through the internal robot visualization of Fig. 9. This Rviz model manages to show almost everything that is going on, as described in the legend table. All frames are expressed as red (x) green (y) blue (z) line segments meeting at the local origin. Spatial force vectors (comprising a force and a torque) are shown as a ray from the local origin (the force) and a bi-vector—a directed plane comprised of four vectors making a square—to represent the torque. Joint torques are represented as pure bi-vectors. Unlike vector descriptions of torque, the bi-vector visualization has an unambiguous scaling relative to the force visualizations, and cannot be confused for them. The four instants pictured in Fig. 9 of the contact transition show the apparent center of pressure moving from the left foot to the right foot, and the corresponding shift in all the joint torques and the predicted reaction forces from the shared body controller. As this is shifting, the reference frame of expression for the sum of reaction forces and the inter-foot task's different of reaction forces swap feet. At all times, the reaction force/torque b.6 representing the sum is roughly equal to the sum ground reaction force calculated without using the passive joints b.4—which means that the robot is supporting the vast majority of its weight even during this transition. The backpack force/torque sensor b.0 confirms this, as it is small (and therefore hard to spot) throughout the transition.

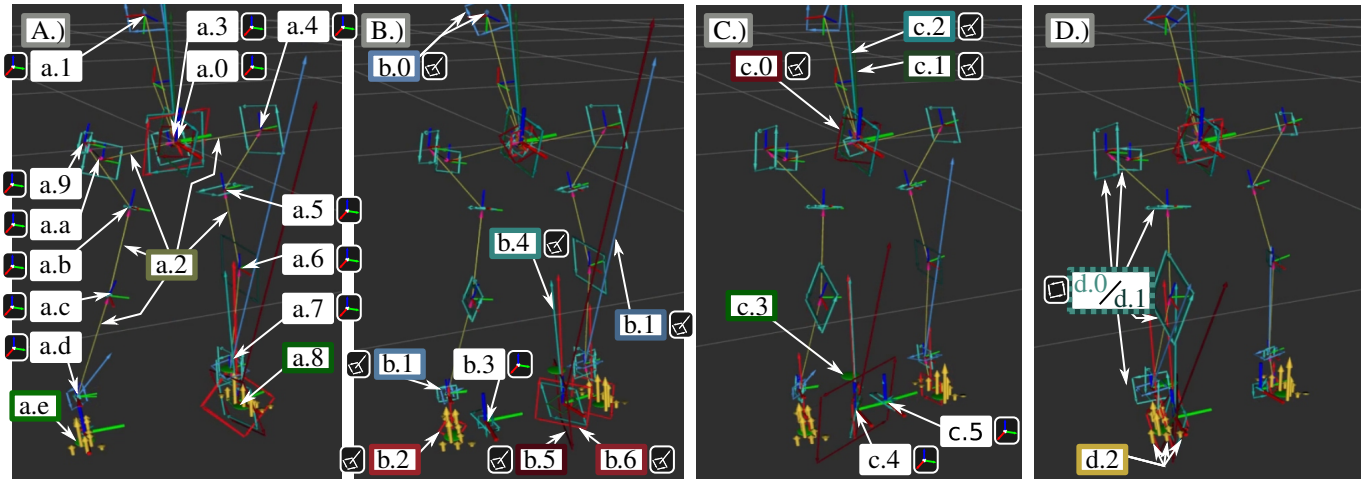

Callout	Description	Callout	Description
a.0	The base or hip frame	b.2	Optimal reaction SFV for the right foot
a.1	The frame of the backpack's force/torque sensor	b.3	Frame of the representation for the difference SFV
a.2	Visualization of child frame to parent frame vectors	b.4	Robot contribution to optimal sum SFV
a.3	(Obscured) frame of the left hip adductor joint	b.5	Measured sum SFV (from structural sensors)
a.9	(Clearly visible) frame of the right hip adductor joint	b.6	Optimal sum SFV
a.4/a.a	Frame of the left/right hip flexor joint	c.0	Measured backpack SFV in hip frame
a.5/a.b	Frame of the left/right passive hip "yaw" joint	c.1	Robot gravity SFV visualization
a.6/a.c	Frame of the left/right knee flexion joint	c.2	Robot gravity compensation SFV visualization
a.7/a.d	Frames of the left/right ankle flexion and passive ankle roll joints (hard to distinguish)	c.3	Measured human COP (ankle origin weighted average)
a.8/a.e	Frame of representation for the constructed sum/difference reaction force vectors—momentarily coincident with the (not visualized) left/right foot bottom frame due to single support	c.4	Frame of rep. for sum SFV
		c.5	Frame of rep. for difference SFV
		d.0	Optimal robot joint torques
		d.1	Applied robot joint torques (filtered and saturated)
b.0	Spatial force vector (SFV) of the backpack force/torque sensor	d.2	Individual FSR relative magnitude visualization for the 12 sensors of each foot, used to estimate within-foot center of pressure
b.1	SFVs of the left and right foot structural force/torque sensors, expressed in the ankle frame		

Fig. 9. Human weight transfer in 0.2 seconds (subfigures evenly spaced in time) showing the exoskeleton visualization in the rviz program.

VII. Discussion

Wearable strength amplification robots are designed to offer humans full control over the superior strength of a robot. In this paper, a frequency domain amplification strategy was introduced and combined with a footstep transition task through a weighted 1-norm shared body control strategy. The strategy's benefits are that it is simple to tune, handles human-led contact transitions, and allows simple rules to determine the priority between tasks in the case of conflicts with torque or contact force limits. This leaves the human in control of both the robot's strength and its force-distribution between the feet. In our brief test, we were able to tune the controller to perform stable amplification and demonstrate a reduction in human torque. While the backdrivable exoskeleton accomplished the majority of the effort reduction through gravity compensation, strength augmentation based on amplification shaping further reduced human effort with respect to unmodeled loads.

Due to the inevitable phase loss in the amplification, we remark that the stability of amplification depends on the damping properties in our model of the human. If we were to replace the operator with a series-elastic mechanical dummy of comparable joint stiffness, we would need to change our human-side compliance strategy to remain stable—introducing damping-like behavior near the point of magnitude crossover. Fortunately, humans appear to be quite cooperative with these aggressive controller designs, as has been noted earlier for controllers based on acceleration feedback [12]—another strategy which increases the human-side compliance of the device.

This controller may be well suited for the capability platform, and manual material handling use cases described in [7]. Its tuning strategy, which involves no direct system identification step, is designed to be practical, and might even be tuned on the fly by the operators themselves—it requires no deep understanding of controls to demand more or less aggressive feedback.

Exoskeletons can be designed for multiple sensor configurations, and in this paper we considered exclusively the configuration where the human–robot interface is sensed. This is hardly the dominant paradigm in exoskeleton mechanical design, as it tends to require a massive exoskeleton. However, amplification shaping could also be achieved with only environment–exoskeleton sensors, as such exoskeletons are also able to distinguish, and therefore control, the human-side and environment-side compliance. This could particularly benefit exoskeletons designed to augment the strength of the elderly and volitional stroke patients, which typically use this sensor configuration to reduce the hardware weight.

APPENDIX A
RELATION TO THE CONTROLLER DESIGN OF [39]

In our own prior work in exoskeleton control, we explored the creation of amplification controllers based on reduction of an "ideal amplification error signal" $Y(s) = (\alpha_0 - 1)F_H(s) - \eta(s)F_A(s)$ (in the notation of Sec. III) using a feedback compensator $G(s)$, with desired actuator force $F_A(s) = G(s)Y(s)$. This left us with a feedback stability model that required system identification of the human. Our proposed structure for $G(s)$ was that of a first order lag filter. The purpose of this section is to explain this prior approach in terms of the modified human-side compliance.

We can eliminate the self-referential $F_A(s)$ definition using algebra:

$$F_A(s) = G(s)((\alpha_0 - 1)F_H(s) - \eta(s)F_A(s)), \tag{44}$$

$$F_A(s) = \frac{G(s)(\alpha_0 - 1)}{(1 + G(s)\eta(s))}F_H(s). \tag{45}$$

We also have a first order lag model of $G(s)$,

$$G(s) = \frac{s + z_G}{s + p_G}k_G, \tag{46}$$

where k_G is the gain, z_G is the zero frequency, and p_G is the pole frequency for the lag. We can therefore express the equivalent $K(s)$ this strategy is implementing,

$$K(s) = \frac{s + z_G}{s/k_G + p_G/k_G + (s + z_G)\eta(s)}(\alpha_0 - 1). \tag{47}$$

From here, we can see that the strategy results in something close to another lag filter (if we neglect the actuator dynamics to treat $\eta(s) \approxeq 1$). However in this case the nominal amplification of the strategy is

$$\alpha(s) = \frac{(\alpha_0 + 1/k_G)s + (\alpha_0 z_G + p_G/k_G)}{(1 + 1/k_G)s + (z_G + p_G/k_G)}, \tag{48}$$

which is similar to the controller parameterization in this paper, but less convenient because its steady state behavior is not α_0 as we might expect but rather $\frac{\alpha_0 + p_G/(k_G z_G)}{1 + p_G/(k_G z_G)}$, which will always be less than α_0. Nor does it return to the natural system behavior at high frequencies, since the nominal value of high frequency $\alpha(s)$ does not return to unity. (In practice it will still return to unity due to $\eta(s)$).

ACKNOWLEDGMENT

For this research in human strength amplification, Apptronik Systems Inc. provided, at no cost, access to their exoskeleton hardware called Sagit-P5. They also provided mechanical maintenance and improvements to the low level interfaces to facilitate the testing. The authors would like to thank Donghyun Kim for providing insights on contact transitions. This system was designed and built by a team including Jonas Fox, Brad Resh, Uday Savaria, Ryan Harkins, Ryan MacWilliams, Joel Cox, and Paul Fleury. The authors would also like to acknowledge Bill Helmsing and Jeff Cardenas for allocating time for our research on the Sagit-P5 exoskeleton.

This work was support in part by NASA grant NNX15AQ33H "Controlling Robots with a Spring in Their Step", for which Gray Thomas is the fellow and Luis Sentis is the advisor.

REFERENCES

[1] H. K. Kwa, J. H. Noorden, M. Missel, T. Craig, J. E. Pratt, and P. D. Neuhaus, "Development of the IHMC mobility assist exoskeleton," in *Robotics and Automation (ICRA), 2009 IEEE International Conference on*. IEEE, 2009, pp. 2556–2562.

[2] O. Harib, A. Hereid, A. Agrawal, T. Gurriet, S. Finet, G. Boeris, A. Duburcq, M. E. Mungai, M. Masselin, A. D. Ames, K. Sreenath, and J. W. Grizzle, "Feedback control of an exoskeleton for paraplegics: Toward robustly stable, hands-free dynamic walking," *IEEE Control Systems Magazine*, vol. 38, no. 6, pp. 61–87, 2018.

[3] T. G. Sugar, J. He, E. J. Koeneman, J. B. Koeneman, R. Herman, H. Huang, R. S. Schultz, D. Herring, J. Wanberg, S. Balasubramanian *et al.*, "Design and control of RUPERT: a device for robotic upper extremity repetitive therapy," *IEEE transactions on neural systems and rehabilitation engineering*, vol. 15, no. 3, pp. 336–346, 2007.

[4] B. Kim and A. D. Deshpande, "An upper-body rehabilitation exoskeleton harmony with an anatomical shoulder mechanism: Design, modeling, control, and performance evaluation," *The International Journal of Robotics Research*, vol. 36, no. 4, pp. 414–435, 2017.

[5] J. Zhang, P. Fiers, K. A. Witte, R. W. Jackson, K. L. Poggensee, C. G. Atkeson, and S. H. Collins, "Human-in-the-loop optimization of exoskeleton assistance during walking," *Science*, vol. 356, no. 6344, pp. 1280–1284, 2017.

[6] S. Lee, J. Kim, L. Baker, A. Long, N. Karavas, N. Menard, I. Galiana, and C. J. Walsh, "Autonomous multi-joint soft exosuit with augmentation-power-based control parameter tuning reduces energy cost of loaded walking," *Journal of Neuroengineering and Rehabilitation*, vol. 15, no. 1, p. 66, 2018.

[7] H. P. Crowell, G. B. Kanagaki, M. P. O'Donovan, C. A. Haynes, J.-H. Park, J. M. Neugebauer, E. R. Hennessy, A. C. Boynton, K. Mitchell, A. J. Tweedell *et al.*, "Methodologies for evaluating the effects of physical augmentation technologies on soldier performance," US Army Research Laboratory Aberdeen Proving Ground United States, Tech. Rep., 2018.

[8] U. A. Training and D. Command, "The us army robotic and autonomous systems strategy," *Fort Eustis (VA): Army Training and Doctrine Command (US)*, 2017.

[9] M. R. Tucker, J. Olivier, A. Pagel, H. Bleuler, M. Bouri, O. Lambercy, J. del R Millán, R. Riener, H. Vallery, and R. Gassert, "Control strategies for active lower extremity prosthetics and orthotics: a review," *Journal of neuroengineering and rehabilitation*, vol. 12, no. 1, p. 1, 2015.

[10] J. Kim, G. Lee, R. Heimgartner, D. Arumukhom Revi, N. Karavas, D. Nathanson, I. Galiana, A. Eckert-Erdheim, P. Murphy, D. Perry, N. Menard, D. K. Choe, P. Malcolm, and C. J. Walsh, "Reducing the metabolic rate of walking and running with a versatile, portable exosuit," *Science*, vol. 365, no. 6454, pp. 668–672, 2019. [Online]. Available: https://science.sciencemag.org/content/365/6454/668

[11] K. Kong and M. Tomizuka, "Control of exoskeletons inspired by fictitious gain in human model," *IEEE/ASME Transactions on Mechatronics*, vol. 14, no. 6, pp. 689–698, 2009.

[12] H. Kazerooni, "Exoskeletons for human power augmentation," in *Intelligent Robots and Systems (IROS), 2005 IEEE/RSJ International Conference on*. IEEE, 2005, pp. 3459–3464.

[13] H. Kazerooni, J.-L. Racine, L. Huang, and R. Steger, "On the control of the berkeley lower extremity exoskeleton (BLEEX)," in *Robotics and Automation (ICRA), 2005 IEEE International Conference on*. IEEE, 2005, pp. 4353–4360.

[14] K. Kong, H. Moon, D. Jeon, and M. Tomizuka, "Control of an exoskeleton for realization of aquatic therapy effects," *IEEE/ASME Transactions on Mechatronics*, vol. 15, no. 2, pp. 191–200, 2010.

[15] G. Lv, H. Zhu, and R. D. Gregg, "On the design and control of highly backdrivable lower-limb exoskeletons: A discussion of past and ongoing work," *IEEE Control Systems Magazine*, vol. 38, no. 6, pp. 88–113, 2018.

[16] J. Lin, G. Lv, and R. D. Gregg, "Contact-invariant total energy shaping control for powered exoskeletons," in *2019 American Control Conference (ACC)*. AACC, 2019, pp. 664–670.

[17] H. Kawamoto and Y. Sankai, "Power assist method based on phase sequence and muscle force condition for hal," *Advanced Robotics*, vol. 19, no. 7, pp. 717–734, 2005.

[18] A. J. Young and D. P. Ferris, "State of the art and future directions for lower limb robotic exoskeletons," *IEEE Transactions on Neural Systems and Rehabilitation Engineering*, vol. 25, no. 2, pp. 171–182, 2016.

[19] W. Yu and J. Rosen, "Neural PID control of robot manipulators with application to an upper limb exoskeleton," *IEEE Transactions on Cybernetics*, vol. 43, no. 2, pp. 673–684, 2013.

[20] M. Fontana, R. Vertechy, S. Marcheschi, F. Salsedo, and M. Bergamasco, "The body extender: A full-body exoskeleton for the transport and handling of heavy loads," *IEEE Robotics & Automation Magazine*, vol. 21, no. 4, pp. 34–44, 2014.

[21] S. C. Jacobsen and M. X. Olivier, "Contact displacement actuator system," September 2014, US Patent 8,849,457.

[22] J. B. Makinson, D. P. Bodine, and B. R. Fick, "Machine augmentation of human strength and endurance Hardiman I prototype project," Specialty Materials Handling Products Operation, General Electric Company, Tech. Rep., 1969.

[23] H. Kazerooni, "Human-robot interaction via the transfer of power and information signals," *IEEE Transactions on Systems, Man, and Cybernetics*, vol. 20, no. 2, pp. 450–463, 1990.

[24] H. Kazerooni and S. Mahoney, "Dynamics and control of robotic systems worn by humans," in *Proceedings. 1991 IEEE International Conference on Robotics and Automation*. IEEE, 1991, pp. 2399–2405.

[25] H. Kazerooni and S. L. Mahoney, "Dynamics and control of robotic systems worn by humans," *Journal of Dynamic Systems, Measurement, and Control*, vol. 113, no. 3, pp. 379–387, 09 1991. [Online]. Available: https://doi.org/10.1115/1.2896421

[26] H. Kazerooni and J. Guo, "Human extenders," *Journal of Dynamic Systems, Measurement, and Control*, vol. 115, no. 2B, pp. 281–290, 1993.

[27] A. Lecours, B. M. St-Onge, and C. Gosselin, "Variable admittance control of a four-degree-of-freedom intelligent assist device," in *Robotics and Automation (ICRA), 2012 IEEE International Conference on*. IEEE, 2012, pp. 3903–3908.

[28] D. J. Gonzalez and H. H. Asada, "Hybrid open-loop closed-loop control of coupled human–robot balance during assisted stance transition with extra robotic legs," *IEEE Robotics and Automation Letters*, vol. 4, no. 2, pp. 1676–1683, 2019.

[29] N. Paine, S. Oh, and L. Sentis, "Design and control considerations for high-performance series elastic actuators," *IEEE/ASME Transactions on Mechatronics*, vol. 19, no. 3, pp. 1080–1091, 2014.

[30] N. A. Paine, "High-performance series elastic actuation," Ph.D. dissertation, The University of Texas at Austin, 2014.

[31] O. H. Campbell, IV, "Framework for full body augmentative exoskeleton control," Master's thesis, The University of Texas at Austin, 2018.

[32] J. E. Colgate and N. Hogan, "Robust control of dynamically interacting systems," *International Journal of Control*, vol. 48, no. 1, pp. 65–88, 1988.

[33] N. Hogan, "Controlling impedance at the man/machine interface," in *Robotics and Automation (ICRA), 1989 IEEE International Conference on*. IEEE, 1989, pp. 1626–1631.

[34] J. E. Colgate and J. M. Brown, "Factors affecting the z-width of a haptic display," in *Robotics and Automation, 1994. Proceedings., 1994 IEEE International Conference on*. IEEE, 1994, pp. 3205–3210.

[35] R. J. Adams and B. Hannaford, "Stable haptic interaction with virtual environments," *IEEE Transactions on Robotics and Automation*, vol. 15, no. 3, pp. 465–474, 1999.

[36] N. Hogan, "Adaptive control of mechanical impedance by coactivation of antagonist muscles," *IEEE Transactions on Automatic Control*, vol. 29, no. 8, pp. 681–690, 1984.

[37] S. P. Buerger and N. Hogan, "Complementary stability and loop shaping for improved human–robot interaction," *IEEE Transactions on Robotics*, vol. 23, no. 2, pp. 232–244, April 2007.

[38] B. He, H. Huang, G. C. Thomas, and L. Sentis, "Complex stiffness model of physical human-robot interaction: Implications for control of performance augmentation exoskeletons," 2019, arXiv preprint arXiv:1903.00704, Accepted at 2019 IEEE International Conference on Intelligent Robots and Systems (IROS) in Macau, China.

[39] B. He, G. C. Thomas, N. Paine, and L. Sentis, "Modeling and loop shaping of single-joint amplification exoskeleton with contact sensing and series elastic actuation," in *2019 Annual American Control Conference (ACC)*. AACC, July 2019, pp. 4580–4587.

[40] G. C. Thomas, J. M. Coholich, and L. Sentis, "Compliance shaping for control of strength amplification exoskeletons with elastic cuffs," in *Proceedings of the 2019 IEEE/ASME International Conference on Advanced Intelligent Mechatronics*. IEEE and ASME, July 2019, pp. 1199–1206.

[41] R. Featherstone, *Rigid body dynamics algorithms*. Springer, 2014.

[42] G. F. Franklin, J. D. Powell, and A. Emami-Naeini, *Feedback control of dynamic systems*. Addison-Wesley Reading, MA, 1994, vol. 3.

[43] G. C. Thomas, J. Mehling, J. Holley, and L. Sentis, "Shaping the compliance of series elastic joints," 2019, unpublished.

[44] T. Koolen, S. Bertrand, G. C. Thomas, T. De Boer, T. Wu, J. Smith, J. Englsberger, and J. Pratt, "Design of a momentum-based control framework and application to the humanoid robot Atlas," *International Journal of Humanoid Robotics*, vol. 13, no. 01, p. 1650007, 2016.

[45] D. Kim, Y. Zhao, G. C. Thomas, B. R. Fernandez, and L. Sentis, "Stabilizing series-elastic point-foot bipeds using whole-body operational space control," *IEEE Transactions on Robotics*, vol. 32, no. 6, pp. 1362–1379, 2016.

[46] D. Kim, S. J. Jorgensen, H. Hwang, and L. Sentis, "Control scheme and uncertainty considerations for dynamic balancing of passive-ankled bipeds and full humanoids," in *2018 IEEE-RAS 18th International Conference on Humanoid Robots (Humanoids)*. IEEE, 2018, pp. 1–9.

[47] L. Sentis, J. Park, and O. Khatib, "Compliant control of multicontact and center-of-mass behaviors in humanoid robots," *Robotics, IEEE Transactions on*, vol. 26, no. 3, pp. 483–501, 2010.

[48] B. J. Stephens and C. G. Atkeson, "Dynamic balance force control for compliant humanoid robots," in *2010 IEEE/RSJ International Conference on Intelligent Robots and Systems*, Oct 2010, pp. 1248–1255.

[49] T. Bretl and S. Lall, "Testing static equilibrium for legged robots," *IEEE Transactions on Robotics*, vol. 24, no. 4, pp. 794–807, 2008.

[50] K. Bouyarmane and A. Kheddar, "On weight-prioritized multitask control of humanoid robots," *IEEE Transactions on Automatic Control*, vol. 63, no. 6, pp. 1632–1647, 2017.

[51] E. J. Candes, M. B. Wakin, and S. P. Boyd, "Enhancing sparsity by reweighted 1 minimization," *Journal of Fourier analysis and applications*, vol. 14, no. 5-6, pp. 877–905, 2008.

[52] G. C. Thomas, "LP Exo: A free implementation of a 1-norm prioritized whole body controller," https://bitbucket.org/gray_thomas/exo_lp.git, 2019.

[53] R. Lougee-Heimer, "The common optimization interface for operations research: Promoting open-source software in the operations research community," *IBM Journal of Research and Development*, vol. 47, no. 1, pp. 57–66, 2003.